Acta Radiologica Open
5(2) 1–6

DOI: 10.1177/2058460115626958
arr.sagepub.com

Spontaneous brain tumor imaging of aged rat by crystal X-ray interferometer-based phase-contrast X-ray CT

Thet-Thet Lwin[1,2], Akio Yoneyama[1,3], Atsuko Hara[2,3], Makoto Ohbu[1,2], Hiroko Maruyama[1,2], Masaya Taguchi[2], Shogo Esashi[2], Tsubasa Matsushima[2], Kei Terazaki[2], Kazuyuki Hyodo[4] and Tohoru Takeda[1,2]

Abstract

Background: Crystal X-ray interferometer-based phase-contrast X-ray computed tomography (C-PCCT) enables the depiction of internal structures of biological tissue without contrast agents.

Purpose: To determine the advantage of this technique in visualizing detailed morphological structures of a rare spontaneous brain tumor in an aged rat.

Material and Methods: An aged rat's spontaneous brain tumor was imaged by C-PCCT without contrast agent. Three-dimensional (3D) images of the tumor microvasculature were reconstructed and compared with pathological pictures.

Results: C-PCCT depicted the tumor's various pathological features clearly, e.g. its cell density and vasculature, and blood clots caused by hemorrhaging and/or hematomas. The obtained images resembled pathological pictures with a magnification of $\times$20 and were used to reconstruct 3D images of the tumor vascularity up to approximately 26 μm in diameter.

Conclusion: Since C-PCCT is able to depict various pathological conditions, it might be useful for cancer research.

Keywords

Crystal X-ray interferometer-based phase-contrast X-ray CT (C-PCCT), computed tomography (CT), aged rat, spontaneous brain tumor

Date received: 15 December 2015; accepted: 20 December 2015

Introduction

The overall incidence of brain tumors, including primary or metastatic malignancies of the central nervous system, is increasing worldwide. Since naturally occurring brain tumors are very rarely used for cancer research, brain tumor models are generated by implanting tumor cells into the brains of mice in most cancer studies. In our laboratory, a rare spontaneous brain tumor was found by chance in a 2-year-old male Wistar rat. In a previous carcinogenicity study involving 11,705 Wistar rats, the incidence of spontaneous nervous system tumors was found to be 2.04%, and most of them occurred in rats age more than 1.5 years (1). Thus, reports about naturally occurring brain tumors in aged rats are very rare.

Various non-invasive imaging techniques have been used to assess the pathophysiology of animal brain tumor models. *In vivo* micro-magnetic resonance imaging depicts brain tumor angiogenesis of small-animal, but its spatial resolution is limited around 60 μm even

[1]Allied Health Sciences, Kitasato University, Sagamihara, Japan
[2]Graduate School of Medical Sciences, Kitasato University, Sagamihara, Japan
[3]Kitasato University, School of Medicine, Sagamihara, Japan
[4]High Energy Accelerator Research Organization, Tsukuba, Japan

Corresponding author:
Thet-Thet Lwin, Allied Health Sciences, Graduate School of Medical Sciences, Kitasato University, 1-15-1 Kitasato, Minami-ku, Sagamihara, Kanagawa, 252-0373 Japan.
Email: thetthet@kitasato-u.ac.jp

with microscopic magnetic resonance angiography (4.7T) using contrast agents (2). Conventional X-ray absorption imaging is often used to assess brain tumors in small animals during biological research (3). However, due to the small absorption differences between biological soft tissues, conventional X-ray absorption imaging techniques cannot depict the internal structures of soft tissue tumors in detail without the use of contrast agents. On the other hand, phase-contrast X-ray technique, in which the phase-shift caused by the sample is utilized to provide image contrast, is approximately 1000 times more sensitive than the conventional absorption X-ray technique (4). Many phase-contrast X-ray imaging techniques such as an interferometry with a crystal X-ray interferometer, grating X-ray interferometer, diffraction enhanced imaging (DEI), and a propagation-based (in-line phase-contrast) method, have been developed. Crystal X-ray interferometric technique detects the phase shift directly, while the other methods detect first or second special gradient of the phase shift. Actually, in comparative experiments among absorption, DEI, grating and crystal X-ray interferometry, the sensitivity was higher, approximately 230 times in crystal X-ray interferometer, approximately 40 times in DEI, and approximately 13 times in grating X-ray interferometer compared to absorption image with monochromatic X-ray of 17.8 keV (5,6). Therefore, crystal X-ray interferometer-based phase-contrast X-ray CT (C-PCCT) enables to depict the internal structures of biological structures, such as amyloid deposits within the brain (7) and cancerous lesions (8,9), in detail. In addition, C-PCCT exhibited higher image quality and contrast than MRI for formalin-fixed cancer lesion (10).

In the present study, the detailed morphological structures of a rare brain tumor that arose spontaneously in an aged rat were clearly depicted using C-PCCT, and the subsequent three-dimensional (3D) image processing revealed the tumor's pathological characteristics.

Material and Methods

Animal preparation

A 2-year-old Wistar male rat (body weight, 500 g) exhibited sudden ataxia of the lower limbs. Thus, the rat was promptly anesthetized via the intraperitoneal injection of sodium pentobarbital (50 mg/kg body weight), and the apex of the left ventricle was surgically cannulated. The rat's blood was then replaced with physiological saline solution containing heparin in order to eliminate blood coagulation artifacts within the rat's blood vessels. An abnormal brain mass containing hemorrhages was seen by chance, so the brain was extracted quickly and fixed using 10% formalin. Non-destructive 3D observation of the sample using C-PCCT was performed before pathological preparation. The experimental protocol was approved by the President of Kitasato University through the judgment of the Animal Care and Use Committee of Kitasato University (approval no. 0402).

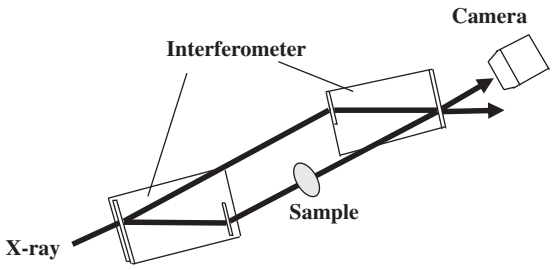

Fig. 1. Schematic picture of the crystal X-ray interferometer-based phase-contrast X-ray CT imaging system.

Phase-contrast X-ray CT imaging system

A two-crystal X-ray interferometer-based phase-contrast X-ray imaging system was used in this study (Fig. 1) (11). An X-ray CCD camera with a 1300×1000 pixel sensor (pixel size, $13 \times 13\,\mu m^2$) and a field of view of $16 \times 13\,mm^2$ was used to detect interference patterns. The spatial resolution determined by Gaussian fit was estimated as about 26 μm. The experiment was performed at the vertical wiggler beamline 14 C of the Photon Factory, Tsukuba, Japan.

During the C-PCCT imaging, the specimen was placed in a 3-cm thick sample cell filled with formalin to prevent the drying of sample. The sample cell was then inserted into the beam path between the mirror and analyzer of the interferometer. The X-ray energy was set at 35 keV. The exposure time was 5 s for each interference pattern, and 250 projections were delivered over 180°. A phase map depicting the spatial distribution of the phase shifts caused by the sample was obtained using a three-step fringe scan. Sectional images were reconstructed by using a filtered back-projection algorithm.

Quantitative image analysis

During the analysis of the C-PCCT images, mass density (ρ) was calculated from a reflective index, which was in turn obtained from the phase shift, Δp, using the following equations:

$$\delta = \Delta p \lambda / 2\pi t \quad (1)$$

$$\rho = 4\pi\delta / \lambda^2 r_e N_A \quad (2)$$

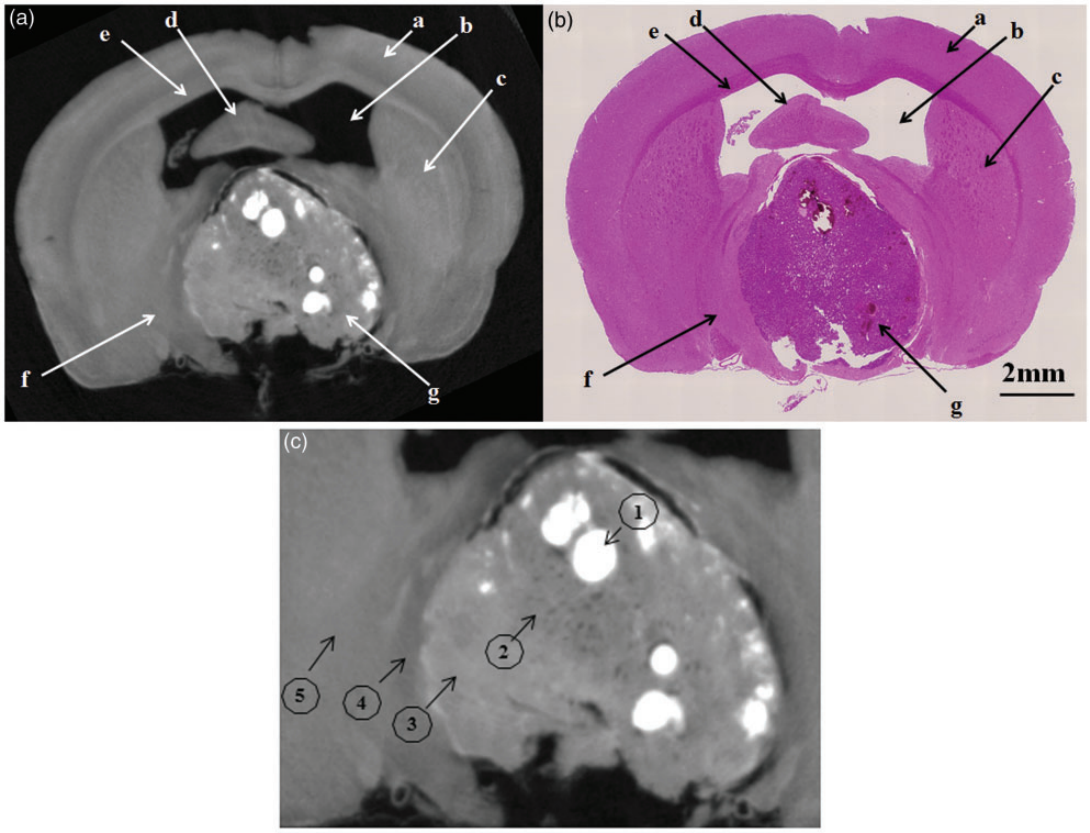

Fig. 2. Coronal section of the rat's brain containing the tumor. (a) Crystal X-ray interferometer-based phase-contrast CT image. (b) Corresponding histological section (H&E stain): a, cortex; b, lateral ventricle; c, caudate putamen; d, hippocampus; e, corpus callosum; f, thalamus; g, tumor. (c) Coronal section of the tumor obtained with crystal X-ray interferometer-based phase-contrast X-ray CT: 1, blood clot-filled blood vessel; 2, inner tumor region; 3, outer tumor region; 4, tumor-surrounding tissue; 5, normal cerebral tissue.

where Δp is the phase shift, δ is the real part of the reflective index, t is the pixel size, λ is the X-ray wavelength, r_e is the classical electron radius, and N_A is Avogadro's number. In addition, calculations of mass density were performed in regions of interest (ROI). Specifically, 10 ROIs were placed in each of the following regions: blood clot-filled vessels; the inner region of the tumor; the outer region of the tumor; the tumor-surrounding tissue; and normal brain tissue.

3D visualization of tumor vessels

Numerical analysis of 3D image data was performed using 3D volume-rending software (Real INTAGE; KGT Inc., Tokyo, Japan). A gray value of 30% was chosen as the threshold for extracting the tumor vascular network.

Histopathological analysis

After the C-PCCT imaging, the brain was embedded in paraffin. Then, 3-μm thick sections were cut in the coronal plane. Hematoxylin-eosin (H&E) staining and immunostaining for a neuronal marker (synaptophysin) were carried out to examine the tumor's histopathological structures. The stained sections were imaged using an optical microscope (Olympus FSX100; Olympus, Tokyo, Japan).

Results

Coronal images of the rat's brain obtained using C-PCCT are shown together with the corresponding pathological sections in Fig. 2a and b. C-PCCT demonstrated excellent tissue conspicuity, and hence, was able to reveal the detailed anatomical structures of the rat's brain, including the cortex, lateral ventricles, caudate putamen, hippocampus, corpus callosum, thalamus, and the tumor, which was located in the brain stem. The tumor was easy to differentiate from the surrounding normal cerebral tissue. A pathological examination based on H&E staining confirmed that the tumor location and cerebral anatomy corresponded to those observed on C-PCCT. Specifically, on C-PCCT, the tumor appeared round, and oval high density structures were seen within it. In addition, the tumor also

Table 1. Absolute density values obtained from crystal X-ray interferometer-based phase-contrast X-ray CT.

	Blood clot-filled vessel	Inner tumor region	Outer tumor region	Tumor -surrounding tissue	Normal cerebral tissue
Density (g/cm^3)	1.157 ± 0.001	1.046 ± 0.01	1.060 ± 0.002	1.051 ± 0.002	1.057 ± 0.001

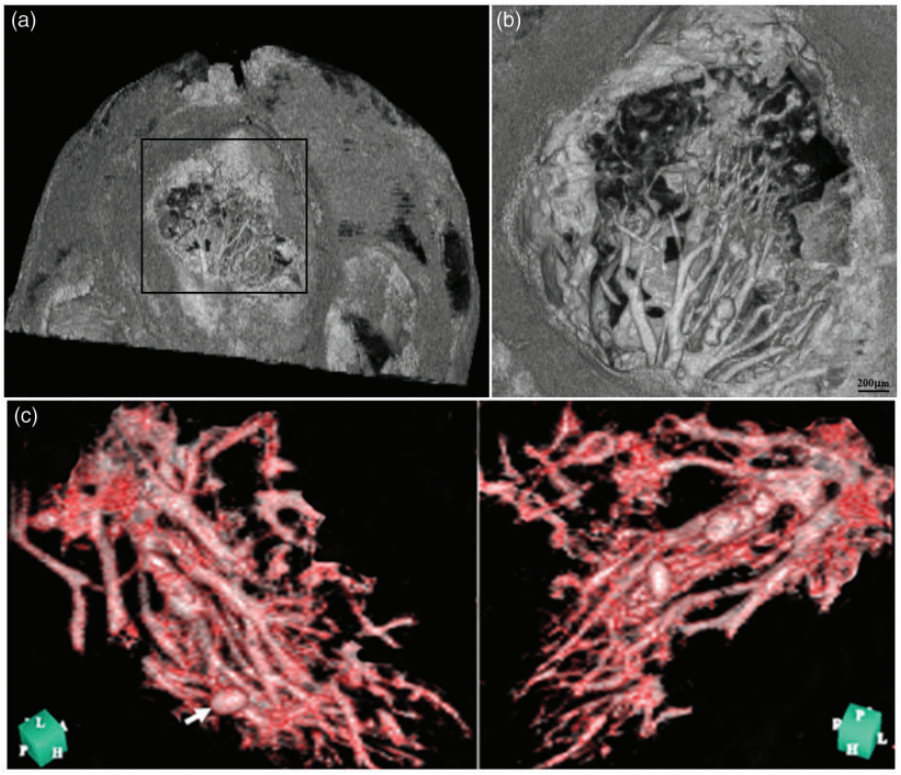

Fig. 3. Three-dimensional reconstruction of the tumor in the rat's brain based on crystal X-ray interferometer-based phase contrast CT images. (a) Overview of the brain and tumor microvasculature. (b) Magnified image of the square region shown in (a). (c) The tumor microvasculature viewed from different angles. The characteristics of the tumor microvasculature were well depicted, e.g. tortuous, saccular (arrow), and dilated blood vessels were observed, which exhibited haphazard patterns of interconnection.

contained small low density duct-like structures, mainly in its inner portion (Fig. 2c). A pathological examination revealed that the high density and small low density structures corresponded to hematoma-derived blood clots/dilated vessels, and hypervascular small vessels that had been perfused with physiological saline, respectively. Marked dilation of the lateral ventricle was also observed. In addition, it was found that a region of the normal cerebral tissue surrounding the tumor, which exhibited a relatively low density, had been affected by edema. Absolute density obtained from C-PCCT images were showed in Table 1.

3D images of the tumor microvessels were reconstructed from the C-PCCT images, as shown in Fig. 3a and b. The 3D images made it possible to view the tumor microvasculature from different angles (Fig. 3c), and the features of these blood vessels were depicted clearly, e.g. tortuous, saccular (arrow), and dilated blood vessels, which exhibited haphazard patterns of interconnection, were observed. Small branch vessels of up to $\sim$26 μm in diameter were clearly visible in the reconstructed images.

In the pathological examination, the tumor displayed high cellularity and hypervascularity. In addition, the tumor cells were round to elongated and possessed hyperchromatic nuclei that exhibited a salt and pepper chromatin pattern and an indistinct cytoplasm. Some of the tumor cells formed Homer-Wright rosettes (H&E stain). Immunostaining demonstrated that the tumor cells were positive for the neuronal marker synaptophysin (Fig. 4a and b).

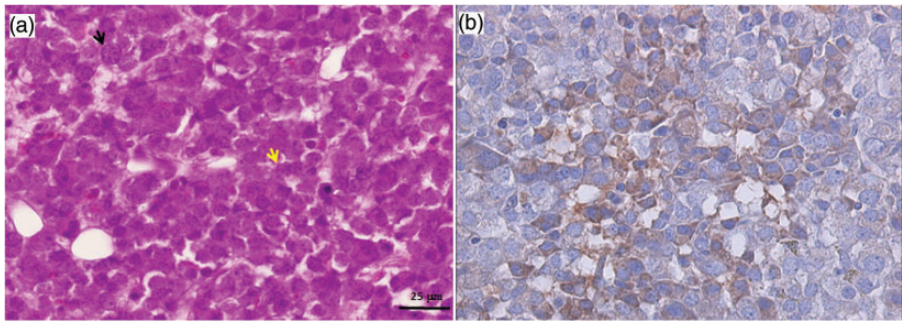

Fig. 4. Pathological section of the tumor. The tumor exhibited high cellularity and vascularity. The tumor cells were round to elongated and possessed hyperchromatic nuclei displaying a salt and pepper chromatin pattern (black arrow) and indistinct cytoplasm. Some of the tumor cells formed Homer-Wright rosettes (yellow arrow). (a) H&E stain. Immunostaining demonstrated that the tumor cells were positive for the neuronal marker synaptophysin (b).

Discussion

A hypervascular tumor that arose spontaneously in an aged rat's brain, was imaged clearly by C-PCCT within formalin solution. The resultant images resembled pathological pictures (magnification ×20), and depicted the tumor's pathological features well. The microvasculature of the rat's brain could be identified well because the formalin solution, with almost the same density of physiological saline, causes high image contrast between formalin within the vessel and the surrounding soft tissues (12). Furthermore, 3D tumor microvasculature of up to ~26 μm in diameter was reconstructed because the image was obtained CT configuration. Tumor vessels were tortuous, dilated, and were connected to each other in a random manner. Grating X-ray phase-contrast imaging was obtained lung metastasis microvasculature of mice at dry stage (13). However, the tissue drying with shrunken and deformity caused unnatural geometry.

In C-PCCT, the gray level of an image corresponds to its absolute density, and the present imaging system has a density resolution of approximately 0.5 mg/cm^3 (5). The absolute densities of the outer parts of the tumor, which contained dense cellular components, and the hypervascular inner region of the tumor were 1.060 g/cm^3 and 1.046 g/cm^3, respectively. Thus, minute density differences caused by tumor cell characteristics and the presence/absence of blood vessels can be distinguished on C-PCCT images without contrast agents. In the present study, blood clots due to hemorrhaging/hematomas exhibited high density, as reported previously (10). Moreover, the absolute density of the tumor-surrounding tissue affected by edema was less dense than the normal cerebral tissue. The dilatation of the left ventricle resulted in hydrocephalus was probably caused by the tumor obstructing the flow of cerebrospinal fluid.

This tumor was pathologically diagnosed as a primary brain tumor of the central nervous system, probably a medulloblastoma. This is the most common type of embryonic brain tumor affecting humans, but such tumors are rarely seen in rats (prevalence, 0.018% in 5480 Wistar rats). In rats, medulloblastoma tend to be seen in younger animals; however, they have also been reported to occur in animals of aged more than 100 weeks in necropsy studies (1).

Intratumoral vessel growth is a hallmark of tumor development, and the inhibition of vessel development is a valid target for anticancer therapy (14). Thus, the ability to visualize intratumoral vessels might be useful for preclinical anticancer research.

The present C-PCCT imaging system is limited to obtaining *in vivo* imaging because of the long image acquisition time. Currently, we are planning to use a new X-ray CCD camera system to perform the high speed data acquisition within 10 min/CT image.

In conclusion, C-PCCT makes it possible to depict the minute pathological structures such as intratumor and its vascular architecture up to approximately 26 μm without the use of contrast agents. Thus, it might be a useful tool for cancer research.

Declaration of conflicting interests

The authors declared no potential conflicts of interest with respect to the research, authorship, and/or publication of this article.

Funding

This research was carried out under the approval (proposal nos. 2009S006, 2012G044, 2013G584) of the committee of the High Energy Accelerator Research Organization and was supported by a grant from Kitasato University School of Allied Health Sciences (Grant-in-Aid for Project, no. 2013-6659).

References

1. Weber K, Garman RH, Germann PG, et al. Classification of neural tumors in laboratory rodents, emphasizing the rat. Toxicol Pathol 2011;39:129–151.

2. Lin CY, Siow TY, Lin MH, et al. Visualization of rodent brain tumor angiogenesis and effects of antiangiogenic treatment using 3D ΔR2-μMRA. Angiogenesis 2013;16: 785–793.
3. Engelhorn T, Eyupoglu IY, Schwarz MA, et al. In vivo micro-CT imaging of rat brain glioma: a comparison with 3T MRI and histology. Neurosci Lett 2009;458:28–31.
4. Takeda T, Momose A, Itai Y, et al. Phase-contrast imaging with synchrotron X-rays for detecting cancer lesions. Acad Radiol 1995;2:799–803.
5. Yoneyama A, Wu J, Hyodo K, et al. Quantitative comparison of imaging performance x-ray interferometric imaging and diffraction enhanced imaging. Med Phys 2008;35:4724–4734.
6. Yoneyama A, Baba R, Hyodo K, et al. Quantitative comparison of performance of absorption, Talbot interferometric, and crystal x-ray interferometric imaging. EPOS^{TM}, ECR 2015. DOI: 10.1594/recr2015/C-0531.
7. Noda-Saita K, Yoneyama A, Shitaka Y, et al. Quantitative analysis of amyloid plaques in a mouse model of Alzheimer's disease by phase-contrast X-ray computed tomography. Neuroscience 2006;138:1205–1213.
8. Momose A, Takeda T, Itai Y, et al. Phase-contrast x-ray computed tomography for observing biological soft tissues. Nat Med 1996;2:473–475.
9. Takeda T, Momose A, Hirano K, et al. Human carcinoma: early experience with phase-contrast x-ray CT with synchrotron radiation: comparative specimen study with optical microscopy. Radiology 2000;214: 298–301.
10. Takeda T, Wu J, Lwin TT, et al. Interferometer-based phase-contrast X-ray computed tomography of colon cancer specimens: Comparative study with 4.74-T magnetic resonance imaging and optical microscopy. J Comput Assist Tomogr 2007;31:214–217.
11. Yoneyama A, Takeda T, Tsuchiya Y, et al. A phase-contrast X-ray imaging system-with a 60×30 mm field of view-based on a skew-symmetric two-crystal X-ray interferometer. Nuclear Instruments and Methods in Physics Research Section A: Accelerators, Spectrometers, Detectors and Associated Equipment 2004;523:217–222.
12. Takeda T, Momose A, Wu J, et al. Vessel imaging by interferometric phase-contrast X-ray technique. Circulation 2001;105:1708–1712.
13. Lin H, Kou B, Li X, et al. Grating-based phase-contrast imaging of tumor angiogenesis in lung metastases. PLoS One 2015;10:e0121438.
14. Weis SM, Cheresh DA. Tumor angiogenesis: molecular pathways and therapeutic targets. Nat Med 2011;17: 1359–1370.